J. Phys. D: Appl. Phys. **46** (2013) 325301 (10pp) doi:10.1088/0022-3727/46/32/325301

# Fabrication of a heterostructure device with Au/PPani–$TiO_2$/ITO configuration and study of device parameters including current conduction mechanism

**Amreen Ara Hussain[1], Arup Ratan Pal[1], Heremba Bailung[1], Joyanti Chutia[1] and Dinkar S Patil[2]**

[1] Physical Sciences Division, Institute of Advanced Study in Science and Technology, Guwahati, Assam, India
[2] Laser and Plasma Technology Division, Bhabha Atomic Research Center, Trombay, Mumbai, India

E-mail: arup_trip@yahoo.com

Received 1 April 2013, in final form 27 June 2013
Published 17 July 2013
Online at stacks.iop.org/JPhysD/46/325301

**Abstract**
Polyaniline based composites incorporating titanium dioxide have been synthesized by an alternative pathway using reactive magnetron sputtering of titanium and plasma polymerization of aniline monomer. Structural, optical and morphological characterizations of plasma polymerized aniline (PPani) and titanium dioxide ($TiO_2$) composites (PPani–$TiO_2$) reveal the evidence for the incorporation of $TiO_2$ in the PPani matrix. A hybrid heterostructure device having PPani–$TiO_2$ composite with a top gold (Au) layer and bottom indium-tin oxide (ITO) layer is fabricated. The developed heterostructure device exhibits rectifying behaviour indicating the formation of a Schottky contact between Au and PPani–$TiO_2$. The detailed electrical measurement of the device is performed under different temperatures. The ideality factor ($n$) and barrier height ($\phi_B$) of the heterojunction diode at room temperature (300 K) are found to be 1.28 and 0.43 eV, respectively. Possible conduction mechanisms are examined using various plotting and curve fitting methods for space charge limited conduction mechanism (SCLC), Schottky emission mechanism and Poole–Frenkel (PF) emission mechanism. The heterostructure device shows best fit of SCLC process as compared to the other mechanisms including Schottky emission and PF emission.

(Some figures may appear in colour only in the online journal)

## 1. Introduction

Electrical conduction in polymer composites has gained immense attention, from both theoretical and experimental points of view [1–4]. Tremendous progress has been made in developing electronic and optoelectronic devices based on conjugated polymer/metal oxides composites such as organic light-emitting diodes, organic thin-film transistors, organic sensors and organic photovoltaics [5–7]. Wide band gap inorganic semiconductors such as ZnO, $TiO_2$, SnO and NiO have excellent electronic, optical and catalytic properties [8–10]. Among the various metal oxides $TiO_2$ has gained much attention because of its properties such as high refractive index, high dielectric constant, high photocatalytic activity, good physical and chemical stability [11, 12]. Furthermore, it is applicable in harvesting solar energy, charge storage, chemical sensors and microelectronic devices [13–15]. Interest in the field of polymer science is constantly paid to conjugated polymers like polyaniline, polythiophene or poly-thiophene derivatives, polypyrrole due to their characteristic optical, electrical and magnetic properties [16]. Polyaniline is a promising conjugated p-type semiconductor with outstanding environmental stability and controlled conductivity through doping/de-doping process [17]. Enormous efforts have also focused on polyaniline based composite materials which are useful in nano device realizations [18, 19]. Synthesis of

 

polyaniline based composite materials with large dielectric constant for development of new generation dynamic random access memories and micro-electromechanical systems has been reported [20].

For developing a heterostructure device using polymer composites, the metal–semiconductor contacts (Schottky contacts) are one of the most important junctions. Most Schottky diodes reported are based on metal (Pt, Al, Au) silicide, however, a number of studies have also dealt with Schottky diodes based on polymer/metal oxide composites. Several research groups have studied the temperature dependent electrical characteristics of Schottky contacts on n-type GaN [21–23]. Very recently, Reddy *et al* [24] reported the $I$–$V$ and $C$–$V$ measurements of Pt/Ru Schottky contacts on n-GaN at various temperatures. Singh *et al* [25] studied metal–polyaniline Schottky junctions where polyaniline is doped with various dopants such as HCl, formic acid and iodine. Kovtyukhova *et al* [26] have reported the wet multilayer assembly of $TiO_2$ or ZnO/polymer composite showing current rectifying behaviour. In addition, Yakuphanoglu *et al* [27] have successfully developed Al/polyaniline Schottky diode and explained the basic diode properties including the barrier height inhomogeneities. The understanding of organic/inorganic heterojunctions and their conduction mechanism is still a subject of interest. The interfacial properties of the metal–semiconductor contacts have a dominant influence on the device performance, reliability and stability.

A great deal of research is concerned with the synthesis of polyaniline composites. Despite the great potential use of polyaniline, the main difficulty remained is its insolubility in common organic solvents. Further, the aggregation of inorganic nanoparticles in the matrix of conjugated polymer also limits the preparation of organic/inorganic composites. Until now the syntheses of organic/inorganic nanocomposites were based on chemical and electrochemical processes as reported by several research groups; however, all of them are multistep processes. In these processes the preparation conditions such as electrolytes and solvents can affect many properties of polyaniline due to which the polymer films decompose rapidly [28]. In recent decades, research work on plasma processes such as sputtering and plasma-enhanced chemical vapour deposition (PECVD) has been carried out throughout the world to explore the applicability of this process for various applications [29–32]. Plasma mediated processes involve both gas phase and surface-assisted reaction mechanisms where the gas phase reactions are initiated by neutrals and charged species. Plasma based techniques provide a solvent free, efficient and versatile way to prepare polymer or polymer composite films for potential use in device engineering. Many literature reports are focused on the plasma polymerization and sputtering of metals; only a few recent reports are found on the concept of a combined process of these two [7, 33].

In this work we present an alternative pathway for the deposition of polyaniline–$TiO_2$ composite films by means of pulsed dc magnetron sputtering and plasma polymerization in a sequential process. The prepared PPani–$TiO_2$ films are characterized and discussed in terms of structural and optical properties. Plasma based method offers an easy route for fabrication of a heterostructure device with the configuration Au/PPani–$TiO_2$/ITO. The measured heterostructure device $I$–$V$ characteristics are used to establish the basic diode parameters like estimating the ideality factor ($n$) and the barrier height ($\phi_B$) at different temperatures. Emphasis is given on the temperature dependent behaviour to investigate the details of current conduction mechanisms.

## 2. Experimental details

### 2.1. Plasma setup

The plasma reactor (Hindhivac, India) consists of a stainless steel chamber of 40 cm in length and 30 cm in diameter placed vertically (figure 1). It is equipped with a water cooled planar magnetron fitted with a titanium target (one inch in diameter, 99.9% purity) and a capacitively coupled planar electrode (9 cm in diameter) placed horizontally below the target. The substrates (Silicon wafers, quartz and micro-glass slides) are placed in the lower powered electrode kept at a distance of 10 cm from the magnetron so that the effect of magnetic field is minimized. A turbo molecular pump (HiPace 300 C) backed by a primary dry pump (Adixen ACP 28G) are used to achieve a base pressure of $2 \times 10^{-5}$ Torr which is measured by a penning gauge (Pfeiffer Vacuum, Full Range Compact Gauge). Initially, argon (Ar) and oxygen ($O_2$) gases are introduced into the plasma reactor at a partial pressure of $4.2 \times 10^{-3}$ Torr where Ar acts as a feed gas for sputtering of titanium and oxygen acts as a reactive gas. Finally, the monomer (aniline, Guaranteed Reagent, Merck, India) vapours are injected into the reactor through a vapour source mass flow controller (VSMFC) as vapour exhausted from the container with liquid aniline partially dipped in a water bath maintained at a temperature of 55 °C and is sprayed through a circular pipe placed around the powered electrode in such a manner that the partial pressure of the reactor is maintained at 0.1 Torr. The working pressure is monitored by a capacitance manometer (Baratron, MKS instruments, USA). For the deposition of polymer/metal oxide composite, an alternately deposited multilayer assembly of plasma polymerized aniline (PPani) and magnetron sputtered titanium in presence of Ar and $O_2$ is performed. RF generator (RF VII, USA) operating at 13.56 MHz is used to facilitate the polymerization process. PPani film deposition is more prominent with low W/FM (W—discharge power, F—gas/monomer flow rate and M—precursor molecular weight) parameter as explained by Debarnot *et al* [31]. Low power and high working pressure, i.e. low W/FM value is maintained for deposition of PPani films where the plasma is energy deficient. This results in low fragmentation of the precursor, thus leading to high retention of conjugated structure in the films. Again, for $TiO_2$ deposition pulsed dc power supply (Pinnacle Plus, Advanced Energy, USA) is used for generation of plasma and sputtering of titanium in presence of Ar and $O_2$ gases only. $TiO_2$ deposition is carried out under low working pressure and high power conditions where the plasma becomes energy efficient. Therefore, with continuous ion bombardment on

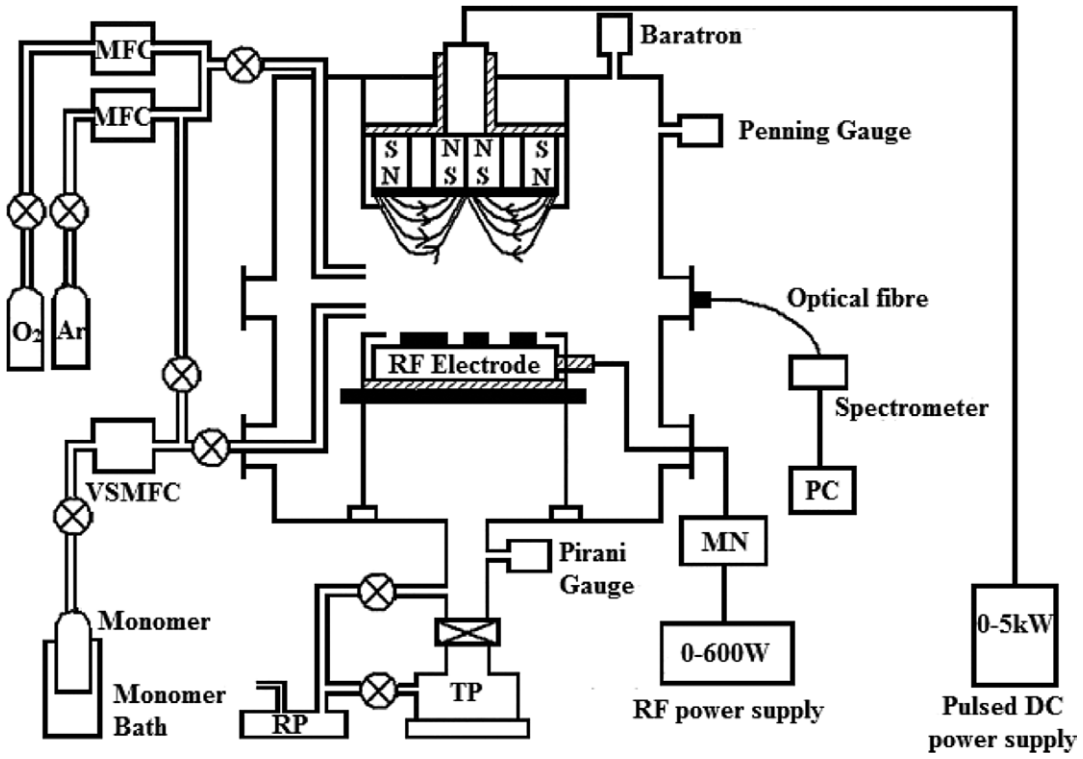


**Figure 1.** Schematic of the plasma reactor for the deposition of PPani–$TiO_2$ composite films. MN—matching network, MFC—mass flow controller, VSMFC—vapour source mass flow controller, TB—turbo molecular pump, RP—rotary pump.

the substrate we get interpenetrating PPani–$TiO_2$ composite film. The total deposition time of PPani–$TiO_2$ composite is 260 s. The various plasma controlling parameters including the deposition time distributions are summarized in table 1(*a*)–(*c*).

Bonding structure of the resulting PPani–$TiO_2$ composite film is determined by FTIR (Nicolet 6700 FT-IR). The FTIR spectrum is measured in the 400–4000 $cm^{-1}$ range working in the transmission mode at normal incidence and averaged over 32 scans. The composite films deposited on silicon wafer are used for FTIR measurements. Ultraviolet–visible (UV–Vis) absorbance is recorded for PPani–$TiO_2$ films deposited on quartz by UV–Vis–NIR Spectrophotometer (UV-1601, Shimadzu, Japan) to study the optical properties of the PPani–$TiO_2$ composite films. Surface morphology is observed using FESEM (Σ IGMA, Zeiss, Germany) and AFM (Digital Instruments, Nanoscope IV). Thickness of the PPani–$TiO_2$ composite film is measured by surface profilometry (Dektak 150, Veeco, USA).

### 2.2. Development of heterostructure device

For device fabrication, the PPani–$TiO_2$ composite is deposited on top of an indium-tin oxide (ITO) coated glass (2.5 cm × 2.5 cm) by a sequential process of plasma polymerization and reactive magnetron sputtering using proper masking arrangement. The PPani–$TiO_2$/ITO configuration is placed in a thermal evaporation chamber where high purity gold (Au) wires under high vacuum of $2 \times 10^{-5}$ Torr are evaporated on the PPani–$TiO_2$/ITO structure. The final heterostructure device has the configuration of Au/PPani–$TiO_2$/ITO with an effective cross sectional area of $2.56 \times 10^{-4}$ $m^2$ and 275 nm thickness. The lateral area of the device is $1.76 \times 10^{-8}$ $m^2$. The temperature dependent heterojunction characteristic in Au/PPani–$TiO_2$/ITO geometry is measured using a potentiostat/galvanostat (Gamry Instruments, USA). All measurements are carried after exposure of the samples in the atmosphere.

## 3. Results and discussions

### 3.1. Structural and morphological properties

The FTIR spectrum of PPani–$TiO_2$ composite is taken on a silicon substrate (figure 2(*a*)). Figure 2(*b*) shows the FTIR transmittance spectra of PPani and $TiO_2$ films. The PPani–$TiO_2$ composite spectrum shows most of the characteristic peaks of emeraldine base (EB) form of polyaniline, thus supporting the formation of polyaniline in the composite film. The appearance of the band at 3372 $cm^{-1}$ is assigned to N–H stretch of secondary amine and the band in the range 3659–3846 $cm^{-1}$ is due to OH stretch of absorbed water [32, 33]. In addition, the bands at 3056 and 2931 $cm^{-1}$ are attributed to unsaturated and saturated C-H stretch which indicates the partial loss of aromaticity during plasma polymerization [34]. Another confirmation of aromaticity is due to the presence of strong intensity bands at 1600 and 1506 $cm^{-1}$ which are assigned to C=C stretch of quinoid and benzenoid units, respectively. Furthermore, the IR absorption spectrum of PPani–$TiO_2$ exhibit an enhanced quinoid to benzenoid band intensity ratio (ratio is 2.78). This result indicates the presence of higher conjugation in polyaniline studied. The peak at 1311 $cm^{-1}$ is attributed to C-N stretch of aromatic ring indicating extended conjugation in the composite

**Table 1.** (*a*) Discharge controlling parameters during the deposition of PPani by RF plasma polymerization (*b*) Discharge controlling parameters during the deposition of $TiO_2$ by reactive magnetron sputtering (*c*) Deposition time distribution for preparing PPani–$TiO_2$ composite.

| Controlling parameters | | Plasma polymerized aniline (PPani) |
|---|---|---|
| (*a*) | | |
| Working pressure (Torr) | | 0.1 |
| Flow rate (sccm) | Argon (Ar) | 30 |
| | Oxygen ($O_2$) | 2 |
| | Aniline | 27 |
| RF power (W) | | 20 |
| Self-bias (V) | | −30 |
| Total deposition time (s) | | 80 |
| Film thickness of each layer (nm) deposited in 20 s | | 46.66 |
| Deposition rate (nm $s^{-1}$) | | 2.33 |
| **Controlling parameters** | | **Titanium dioxide ($TiO_2$)** |
| (*b*) | | |
| Working pressure (Torr) | | $4.2 \times 10^{-3}$ |
| Flow rate (sccm) | Argon (Ar) | 30 |
| | Oxygen ($O_2$) | 2 |
| Pulsed dc power (W) | | 35 |
| Frequency (kHz) | | 100 |
| Reverse time ($\mu$s) | | 4.5 |
| Discharge voltage (V) | | 208 |
| Discharge current (mA) | | 170 |
| Total deposition time (s) | | 180 |
| Film thickness of each layer (nm) deposited in 60 s | | 29.33 |
| Deposition rate (nm $s^{-1}$) | | 0.49 |
| **Layers** | **PPani (s)** | **$TiO_2$ (s)** |
| (*c*) | | |
| 1 | 20 | — |
| 2 | — | 60 |
| 3 | 20 | — |
| 4 | — | 60 |
| 5 | 20 | — |
| 6 | — | 60 |
| 7 | 20 | — |

*Note:* Total deposition time: 260 s.

film [35]. The strong absorption at 1103 $cm^{-1}$ is due to in-plane C–H deformation. The absorption band at 2217 $cm^{-1}$ is due to the C≡N stretch of nitrile group leading to possible chain termination under the plasma environment. Further, the bands at 750 $cm^{-1}$ due to 1, 2 di-substituted aromatic ring (ortho) and 696 $cm^{-1}$ due to 1, 3 di-substituted aromatic ring (meta) suggests crosslinking in PPani [36]. Moreover, the sputtered $TiO_2$ has absorption at 723, 530 and 671 $cm^{-1}$ which is the characteristic peaks of $TiO_2$ and are assigned to antisymmetric Ti–O–Ti mode of $TiO_2$, Ti–OH and Ti–O stretch [8, 37, 38]. According to Andrés *et al* [39] peak at 671 $cm^{-1}$ is due to silicon substrate correction so that it will not be taken into consideration. It is observed that most of the absorption band positions of PPani–$TiO_2$ are shifted when compared with the spectra of pure PPani films and conventionally prepared Pani-$TiO_2$ films [35, 40]. This suggests the strong interaction between PPani and the oxide ($TiO_2$) surface associated with the interaction of titanium and nitrogen atom in PPani. Since titanium is a transition metal and titanium has an intense tendency to form coordination compound with nitrogen atom in polyaniline, such adhesion will not only constrain the motion of polyaniline chains but also restricts the mode of vibration in polyaniline. Thus, the strong interaction causes the shifting of bands with appearance of some new bands. Moreover, the action of hydrogen bonding between $TiO_2$ and polyaniline is also contributory to the shifting of bands [41].

Surface morphology of PPani–$TiO_2$ hybrid samples is shown in figure 3(*a*). The PPani–$TiO_2$ composite film shows a very smooth surface on the micrometre scale, with very few sub-micrometre droplets [42]. Figures 3(*b*)–(*d*) show the AFM images (2D, 3D and phase images, scale 1 $\mu$m × 1 $\mu$m) of PPani–$TiO_2$ composite film. The morphological features of the surface represent a very uniform structure with an AFM rms surface roughness of 0.36 nm. The heterostructure device performance mainly relies on the structure, morphology and interfacial contact. Since the SEM and AFM micrographs of PPani–$TiO_2$ composite show a very smooth and uniform film, a better interfacial contact is expected in the heterostructure device.

### 3.2. *Optical properties*

To understand the absorption and optical properties, UV–Vis spectroscopy of PPani–$TiO_2$ composite films are examined.

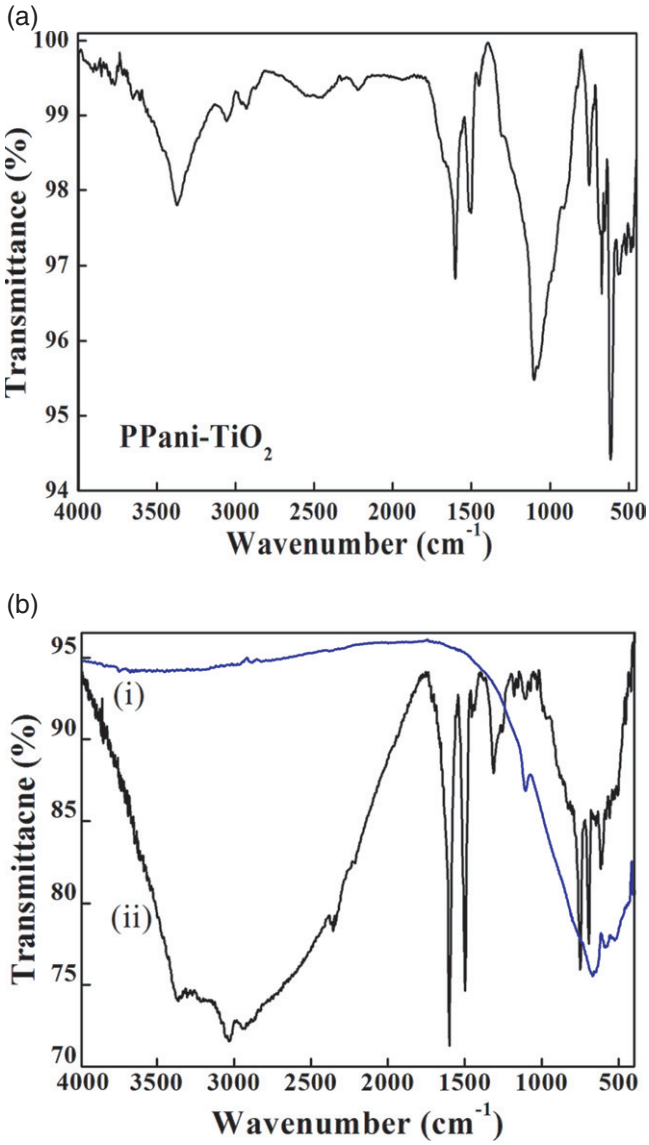


**Figure 2.** (*a*) FTIR transmittance spectrum of PPani–$TiO_2$ composite film (*b*) FTIR transmittance spectra of (i) sputtered $TiO_2$ film and (ii) PPani film.

Figure 4 shows the UV–Vis absorbance spectra of PPani–$TiO_2$ composite. Three absorption peaks at 201, 244 and 296 nm are observed and are consistent with the literature reports on polyaniline base. These bands are assigned to $\pi \rightarrow \pi^*$ transition of benzene ring [40]. Considerable blue shift in the absorption bands is observed in the PPani–$TiO_2$ composite when compared with the reported results in polyaniline base [35, 43]. This noticeable blue shift is ascribed to the bonding and interaction between $TiO_2$ and quinoid unit of PPani due to hydrogen bonding in the form of NH··O–Ti in PPani–$TiO_2$ composite [44]. A little hump in the wavelength region 400–430 nm is observed, which is attributed to polaron-$\pi^*$ transition [38]. This indicates that the insertion of $TiO_2$ has affected the polymer chain owing to strong interaction at the interface of PPani and $TiO_2$. In the inset the transmittance UV–Vis spectrum is shown. It is remarkable to note that the transmittance of PPani/$TiO_2$ composite film is considerably enhanced in the visible region. The high transmittance indicates smooth surfaces and relatively good film homogeneity which is also confirmed from the FESEM and AFM micrographs [45].

### *3.3. Electrical properties*

The typical $I$–$V$ characteristics of Au/PPani–$TiO_2$/ITO heterostructure diode at different temperatures are shown in figure 5 which exhibits a rectifying behaviour originated by the formation of a Schottky contact between Au and PPani–$TiO_2$ composite in Au/PPani–$TiO_2$/ITO heterostructure diode. It is reported that schottky barrier diodes at room temperature alone does not give detailed information about their conduction process. Therefore, analysis of diode parameters at different temperatures allows us to understand different aspects of barrier formation and charge transport mechanism. In order to attain an insight of the heterostructure diode characteristics, the standard thermionic emission (TE) model of a Schottky junction is used [46].

The $I$–$V$ characteristics for the Schottky diode are analysed by the following relation [27, 47, 48]:

$$I = I_o \exp\left(\frac{e_o V_c}{n k_B T}\right) - 1, \tag{1}$$

$$I_o = A A_R^{**} T^2 \exp\left(\frac{-\phi_B^{eff}}{k_B T}\right), \tag{2}$$

where $I$ is the current flowing, $I_o$ is the saturation current, $V_c$ is the voltage drop across contact, $e_o$ is the electronic charge, $T$ is the temperature, $n$ is the ideality factor, $k$ is the Boltzmann constant ($8.62 \times 10^{-5}$ eV $K^{-1}$), $A$ is the diode area, $A_R^{**}$ is the Richardson constant and $\phi_B^{eff}$ is the effective |Schottky barrier height.

The saturation current ($I_o$) is obtained by extrapolating the linear portion of ln $I$ versus $V$ plot (figure 6) to zero bias and the diode ideality factor is calculated from the slope of the linear portion of the ln $I$ versus $V$ plot as follows:

$$n = \left(\frac{e_o}{kT}\right)\left(\frac{\partial V_c}{\partial \ln I}\right). \tag{3}$$

The ideality factor ($n$) for an ideal diode is 1 but it may vary from 1 to 2 depending upon the fabrication process and choice of the semiconducting material. Higher values of the ideality factor leads to nonideality which can be attributed to the presence of interfacial native oxide layer, barrier inhomogeneity, generation recombination currents and surface states [3, 24].

Similarly, the barrier height and the Richardson constant is determined from equation (2) using the Richardson plot [47]. Figure 7 shows the variation of $\ln(I_o/T^2)$ against $1000/T$. The Richardson constant ($A_R^{**}$) should depend on the effective mass of the charge carriers, which determines the mobility of carrier transport in the heterostructure device. Hence, the value of $A_R^{**}$ is determined from intercept of the $\ln(I_o/T^2)$ versus $1000/T$ plot. The calculated value of $A_R^{**}$ is $7.96 \times 10^{-6}$ A $cm^{-2}$ $K^{-2}$. This value is significantly lower than the known value of Richardson constant for free electron (120 A $cm^{-2}$ $K^{-2}$) implying inhomogeneous barrier heights

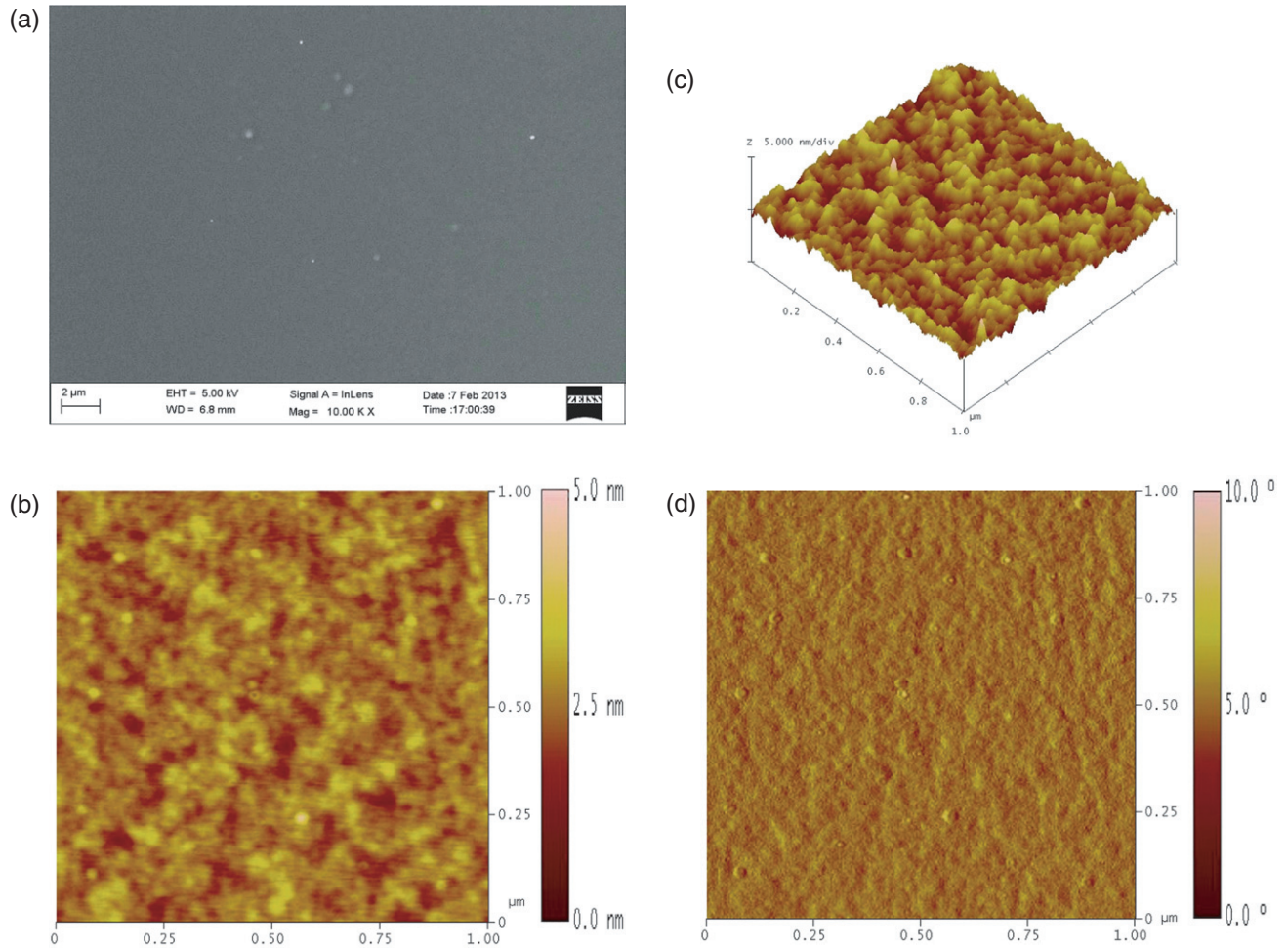


**Figure 3.** (*a*) Surface FESEM image of PPani–$TiO_2$ composite film. (*b*), (*c*) 2D and 3D AFM topographies of PPani–$TiO_2$ composite film (*d*) Phase image of PPani–$TiO_2$ composite film.

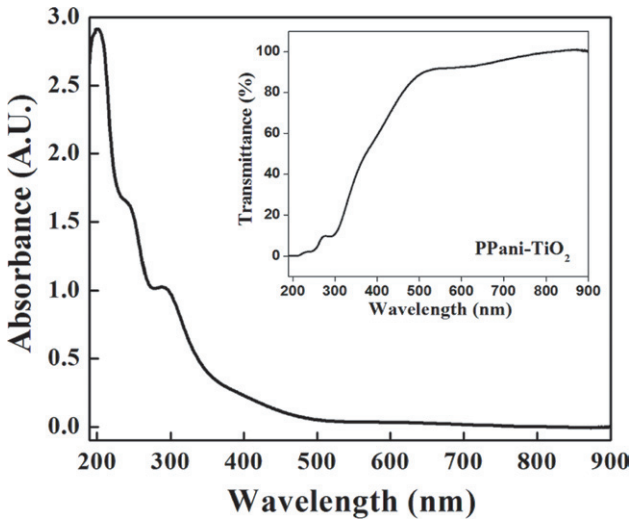


**Figure 4.** UV–Vis absorbance spectrum of PPani–$TiO_2$ composite film. In the inset, the transmittance spectrum of the PPani–$TiO_2$ composite film is shown.

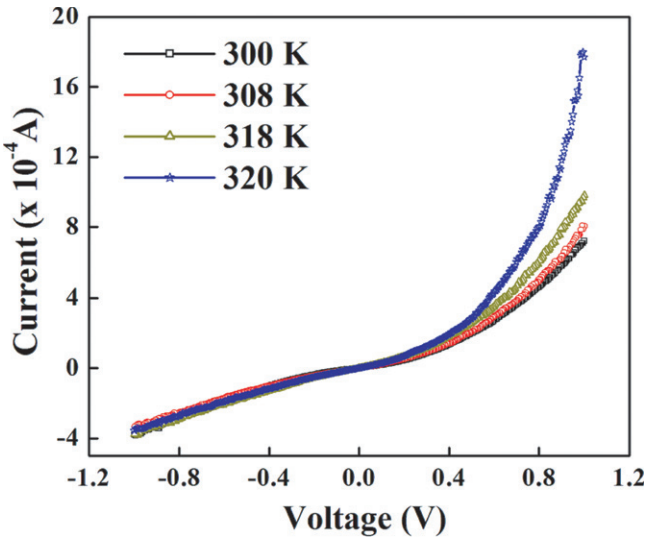


**Figure 5.** *I*–*V* characteristics of the Au/PPani–$TiO_2$/ITO heterostructure diode at different temperatures.

and potential fluctuations at the interface consisting of low and high barrier areas [3, 48]. Therefore, the current of the diode might flow preferentially through the lower barriers in the potential distribution. Thus the value of Richardson constant is affected by inhomogeneity of the barrier. This discrepancy of the lower value of Richardson constant can be corrected and described by using Tung's model [49] i.e. considering an effective area lower than the geometric area of the diode.

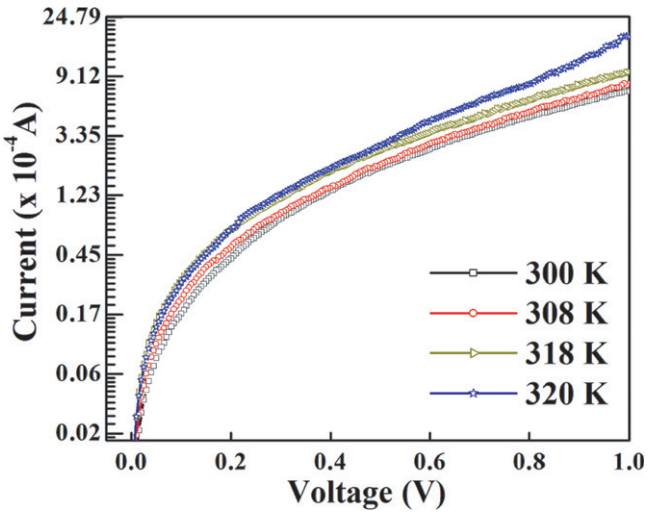


**Figure 6.** Forward current characteristics of Au/PPani–$TiO_2$/ITO heterostructure diode at different temperatures.

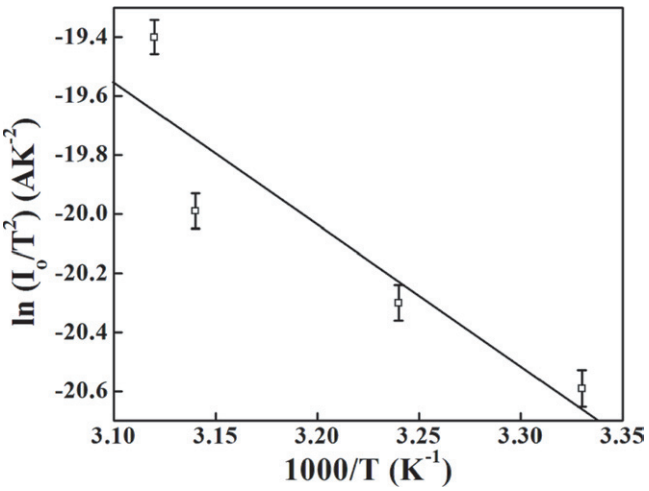


**Figure 7.** Richardson plot of $\ln(I_o/T^2)$ versus *1000/T* for Au/PPani–$TiO_2$/ITO heterostructure diode.

Finally, the barrier height is calculated from the relation:

$$\phi_B = \frac{kT}{e_o} \ln\left(\frac{AA_R^{**}T^2}{I_o}\right). \quad (4)$$

The determined $n$ and $\phi_B$ values from equation (3) and (4) are presented in figure 8 as a function of temperature. It is seen from the figure that the values of barrier height increase and ideality factor decreases with increase in temperature. The ideality factor is indicative of the interface uniformity [2]. The ideality factor close to one indicates that the TE mechanism is dominant [24]. On the other hand, the obtained ideality factor being nearly equal to one is due to uniformity and homogeneity of the interface structure which is well expected from the FESEM and AFM micrographs showing quite homogeneous film. However, in spite of the almost ideal behaviour of the contact observed at temperature 308 K ($n = 1.05$) and above, the deviation from the ideality observed at low temperature condition ($n = 1.28$) suggests that an inhomogeneous barrier has actually formed. This change in the ideality factor and barrier height at different temperatures

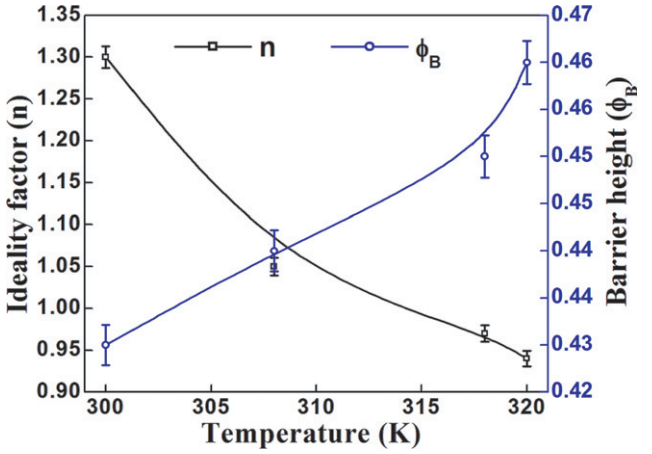


**Figure 8.** Ideality factor and barrier height as a function of temperature.

can be explained according to barrier height inhomogeneity. In the model developed by Tung [48, 49] of inhomogeneous contact, the small regions, so called 'patches', with lower barrier height embedded in a uniform high barrier background were assumed to exist in the junction. These patches may result from atomic inhomogeneities such as defects or from high electric field at the edge of the diode. The area of these patches is smaller than the total area of the diode (diode lateral area, $1.76 \times 10^{-8}$ m$^2$). Thus, it is assumed that the junction's interface contains small local regions with barrier height of 0.429 eV at 300 K and 0.46 eV at 320 K through which charge carriers can flow. Since current transport across the metal–semiconductor interface is a temperature dependent process, therefore, under this condition, at higher temperatures the current transport is dominated by the uniform barrier while at lower temperature, the presence of inhomogeneities with lower barrier heights becomes dominant.

Further, In order to understand the $I$–$V$ relations in conjunction with the structural evolution of PPani–$TiO_2$ composite materials as a function of temperature, the analysis of conduction mechanism is essential. The temperature dependent barrier characteristics of the Au/PPani–$TiO_2$/ITO heterostructure diode is interpreted on the basis of three conduction mechanisms, field-enhanced Schottky emission ($I_S$) mechanism, Poole–Frenkel (PF) emission ($I_{PF}$) mechanism and space charge limited conduction (SCLC) mechanism. As is already known, the Schottky emission mechanism is an electrode limited conduction generally occurring at low voltages at which the electrons on the surface of the injecting electrode transit above the potential barrier [50]. PF emission mechanism on the other hand, is a bulk limited conduction that arises due to field-enhanced thermal excitation of trapped electrons into the insulator conduction band [51, 52]. Both of these emissions result from the coulomb lowering of the potential barrier under an applied electric field and are expressed as [46, 51, 52]

$$J_S = AT^2 \exp\left(\frac{e_o}{kT}\sqrt{\frac{e_o E}{4\pi\varepsilon_o\varepsilon}} - \frac{e_o\phi_S}{kT}\right) \quad (5)$$

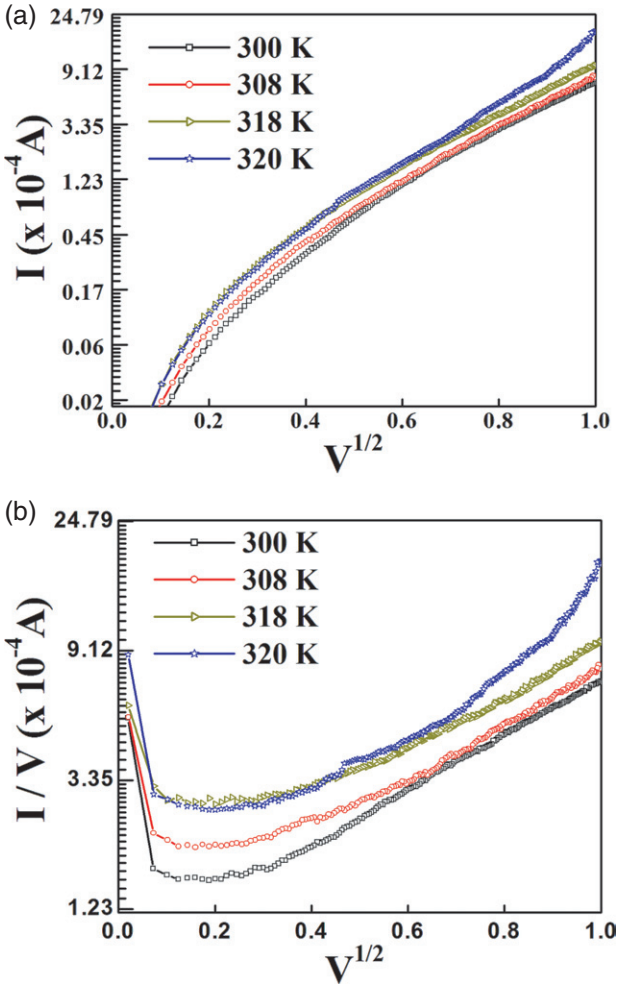


**Figure 9.** The plots of (*a*) $\ln(I)$ versus $V^{1/2}$ (*b*) $\ln(I/V)$ versus $V^{1/2}$ representing Schottky emission mechanism and PF emission mechanism.

for Schottky emission,

$$J_{\mathrm{PF}} = BE\exp\left(\frac{e_{\mathrm{o}}}{kT}\sqrt{\frac{e_{\mathrm{o}}E}{\pi\varepsilon_{\mathrm{o}}\varepsilon}} - \frac{e_{\mathrm{o}}\phi_{\mathrm{PF}}}{kT}\right) \tag{6}$$

for PF emission, where A and B are constants, $\varepsilon_{\mathrm{o}}$, $\varepsilon$, $e_{\mathrm{o}}$, $E$, $k$ and $T$ are permittivity in vacuum, dielectric constant, electronic charge, electric field, Boltzmann constant and temperature in Kelvins, respectively. $\phi_{\mathrm{S}}$ is the barrier height for the injecting electron for Schottky emission while $\phi_{\mathrm{PF}}$ is the barrier for the trapped electrons for PF emission.

Figure 9 has the $I$–$V$ plots from figure 5 converted to $\ln I$ versus $V^{1/2}$ for Schottky emission and $\ln(I/V)$ versus $V^{1/2}$ for Poole–Frenkle emission. The slopes ($m$) for the linear regions in the plots can be obtained as:

$$m_{\mathrm{S}} = \beta/2kT \qquad \text{for Schottky emission,}$$
$$m_{\mathrm{PF}} = \beta/kT \qquad \text{for Poole–Frenkel emission,}$$

where $\beta = \sqrt{e_{\mathrm{o}}^3/\pi\varepsilon_{\mathrm{o}}\varepsilon}$. Using this equation $\beta$ can be theoretically calculated from the dielectric constant. The $\beta$ values for each mechanism are calculated based on the slope of the linear region. The calculated $\beta$ values are summarized in table 2. The $\beta$ values for Schottky and Poole–Frenkel emissions are too big compared to the theoretical value ($2.8 \times 10^{-5}$ eV/(V m)$^{1/2}$) calculated based on the dielectric constant of the composite material. Again, figures 9(*a*) and (*b*) show the semi-logarithmic plots of $\ln I$ versus $V^{1/2}$ and $\ln(I/V)$ versus $V^{1/2}$. Both the plots should be linear for a Schottky emission mechanism and PF emission mechanism, but none of the plots shows a linear relationship. Therefore, this indicates that none of the two processes could be a major conduction mechanism. Further, the current and voltage relationship for SCLC is explained from the power law or the Child–Langmuir law expressed as [1, 53]

**Table 2.** $\beta$-values evaluated from the plots according to Schottky (S) and Poole–Frenkel (PF) models for the heterostructure diode at different temperatures.

| Temperature (K) | $\beta_{\mathrm{S}}$ | $\beta_{\mathrm{PF}}$ |
|---|---|---|
| 300 | $7.84 \pm 0.04$ | $2.90 \pm 0.02$ |
| 308 | $11.96 \pm 0.09$ | $3.50 \pm 0.05$ |
| 318 | $12.54 \pm 0.09$ | $4.00 \pm 0.09$ |
| 320 | $14.89 \pm 0.07$ | $5.83 \pm 0.081$ |

*Note*: $\beta$-value unit: $\times 10^{-5}$ eV/(V/m)$^{1/2}$.

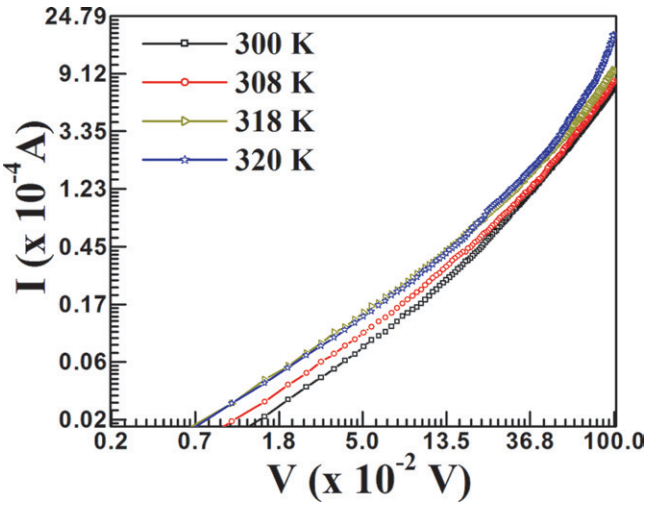


**Figure 10.** The plot of $\ln(I)$ versus $\ln(V)$ representing SCLC mechanism.

$$J = AE^{\alpha}, \tag{7}$$

where $J$ is the current density, $A$ is a constant, $E$ is the applied field and $\alpha$ is a constant, $\alpha = 1$ for ohmic behaviour, $\alpha = 2$ for an insulator without or with shallow traps and $\alpha > 2$ for traps distributed in energy. Figure 10 shows the plot of $\ln I$ versus $\ln V$ that exhibits a good linear relationship as compared to the plots of $\ln I$ *versus* $V^{1/2}$ and $\ln(I/V)$ *versus* $V^{1/2}$ for Schottky and PF emission mechanisms. For comparing the linearity of the heterostructure diode, linear regression is performed. The R squared values and residual variance values are presented in table 3. It is known that, for an ideal linear fitting the R squared values and residual variance values should be 1 and 0, respectively. Fortunately, all the R squared values and residual variance values listed in the table are close to the ideal values indicating good

**Table 3.** R-squared values and residual variances for the linear fitting for the space charge limited current (SCLC) mechanism at different temperatures.

| Temperature (K) | R-squared | Residual variance |
|---|---|---|
| 300 | 0.96164 | 0.209 |
| 308 | 0.96459 | 0.20019 |
| 318 | 0.96884 | 0.18766 |
| 320 | 0.94151 | 0.25743 |

agreement of the SCLC conduction mechanism. Thus, SCLC mechanism shows the best fit compared to other mechanisms including Schottky emission and PF emission mechanisms.

## 4. Conclusion

In this paper, we have demonstrated an alternative pathway for the synthesis of an organic/inorganic based composite material (PPani–$TiO_2$) by reactive magnetron sputtering and plasma polymerization in a sequential process. We are able to show evidence for the presence of $TiO_2$ in the film by FTIR, FESEM and UV–Vis studies. Because of the tendency to form coordination compound between titanium and nitrogen in PPani macromolecule, the incorporation of $TiO_2$ in PPani matrix is confirmed from FTIR and UV–Vis spectra. The morphological investigations using FESEM and AFM present a smooth and uniform PPani–$TiO_2$ composite film. The results also indicate that the main characteristics of the PPani–$TiO_2$ composites are not affected by the plasma route presented for synthesis of PPani–$TiO_2$. Moreover, the prepared films are stable upon hours of exposure to atmosphere. In addition, we are also successful in using these composite films for developing a heterostructure device with configuration Au/PPani–$TiO_2$/ITO. The device shows a rectifying behaviour indicating the formation of a Schottky contact between Au and PPani–$TiO_2$. The basic diode parameters are extracted from the $I$–$V$ measurements based on the standard thermionic emission model. The diode ideality factor and Schottky barrier height at room temperature are 1.28 and 0.43 eV, respectively. Further, the conduction mechanism in the heterostructure diode is governed by space charge limited conduction mechanism rather than Schottky emission mechanism or Poole–Frenkel emission mechanism. This is due to nonlinear relationship of the plots of $\ln(I)$ versus $V^{1/2}$ and $\ln(I/V)$ versus $V^{1/2}$. It is concluded that the development of PPani–$TiO_2$ composite heterostructure device prepared by plasma based route demonstrates an easy, single step and new technique for preparing stable hybrid materials which is promising for advanced device realizations.

## Acknowledgments

Authors gratefully acknowledge the financial supported from BRNS-DAE, Government of India (Grant No 2009/34/45/BRNS/3327). We thank IIT-Guwahati and IIT-Bombay for providing some of the sample characterization facilities.

## References

[1] Yoo K H, Kang K S, Chen Y, Han K J and Kim J 2008 *Nanotechnology* **19** 505202
[2] Yakuphanoglu F 2007 *J. Phys. Chem.* C **111** 1505
[3] Mahmoud W E 2009 *J. Phys. D: Appl. Phys.* **42** 155502
[4] Ameen S, Song M, Kim D-G, Im Y-B, Seo H-K, Kim Y S and Shin H-S 2012 *Macromol. Res.* **20** 30
[5] Sarma B K, Pal A R, Bailung H and Chutia J 2012 *J. Phys. D: Appl. Phys.* **45** 275401
[6] Tanaka H, Yasuda T, Fujita K and Tsutsui T 2006 *Adv. Mater.* **18** 2230
[7] Sharma S, Pal A R, Chutia J, Bailung H, Sarma N S, Dass N N and Patil D 2012 *Appl. Surf. Sci.* **258** 7897
[8] Yoo D, Kim I, Kim S, Hahn C H, Lee C and Cho S 2007 *Appl. Surf. Sci.* **253** 3888
[9] Meybodi S M, Hosseini S A, Rezaee M, Sadrnezhaad S K and Mohammadyani D 2012 *Ultrason. Sonochem.* **19** 841
[10] Lin W-C, Shih C-J, Wu C-C and Seshia A A 2013 *IEEE Trans. Nanotechnol.* **12** 21
[11] Ahn Y U, Kim E J, Kim H T and Hahn S H 2003 *Mater. Lett.* **57** 4660
[12] Tang H, Prasad K, Sanjinès R, Schmid P E and Lévy F 1994 *J. Appl. Phys.* **75** 2042
[13] Zheng Q, Zhou B, Bai J, Li L, Jin Z, Zhang J, Li J, Liu Y, Cai W and Zhu X 2008 *Adv. Mater.* **20** 1044
[14] Lin Z, Jiang C, Zhu C and Zhang J 2013 *Appl. Mater. Interfaces* **5** 713
[15] Aluri G S, Motayed A, Davydov A V, Oleshko V P, Bertness K A, Sanford N A and Mulpuri R V 2012 *Nanotechnology* **23** 175501
[16] Huang W S and MacDiarmid A G 1993 *Polymer* **34** 1833
[17] Lux F 1994 *Polymer* **35** 2915
[18] Khan A A and Khalid M 2010 *J. Appl. Polym. Sci.* **117** 1601
[19] Nabid M R, Golbabaee M, Moghaddam A B, Dinarvand R and Sedghi R 2008 *Int. J. Electrochem. Sci.* **3** 1117
[20] Dey A, De S, De A and De S K 2004 *Nanotechnology* **15** 1277
[21] Zhou Y, Wang D, Ahyi C, Tin C-C, Williams J, Park M, Williams N M, Hanser A and Preble E A 2007 *J. Appl. Phys.* **101** 024506
[22] Ravinandan M, Rao P K and Reddy V R 2009 *Semicond. Sci. Technol.* **24** 035004
[23] Horváth Zs J, Dobos L, Beaumont B, Bougrioua Z and Pécz B 2010 *Appl. Surf. Sci.* **256** 5614
[24] Reddy N N K and Reddy V R 2012 *Bull. Mater. Sci.* **35** 53
[25] Singh R, Srivastava D N and Singh R A 2001 *Synth. Met.* **121** 1439
[26] Kovtyukhova N I, Martin B R, Mbindyo J K N, Smith P A, Razavi B, Mayer T S and Mallouk T E 2001 *J. Phys. Chem.* B **105** 8762
[27] Yakuphanoglu F and Şenkal B F 2007 *J. Phys. Chem.* C **111** 1840
[28] Gray F M 1997 *Polymer Electrolytes* (*RSC Materials Monographs*) (Cambridge, UK: The Royal Society of Chemistry)
[29] Hoppe H and Sariciftci N S 2004 *J. Mater. Res.* **19** 1924
[30] Choi K-H, Jeong J-A, Kang J-W, Kim D-G, Kim J K, Na S-I, Kim D-Y, Kim S-S and Kim H-K 2009 *Sol. Energy Mater. Sol. Cells* **93** 1248
[31] Debarnot D, Mérian T and Poncin-Epaillard F 2011 *Plasma Chem. Plasma Process.* **31** 217
[32] Paterno L G, Manolache S and Denes F 2002 *Synth. Met.* **130** 85
[33] Pal A R, Sarma B K, Adhikary N C, Chutia J and Bailung H 2011 *Appl. Surf. Sci.* **258** 1199
[34] Zhao B, Hu H and Haddon R C 2004 *Adv. Funct. Mater.* **14** 71
[35] Sarma B K, Pal A R, Bailung H and Chutia J 2011 *Plasma Chem. Plasma Process.* **31** 741

[36] Cruz G J, Morales J, Castillo-Ortega M M and Olayo R 1997 *Synth. Met.* **88** 213
[37] Pawar S G, Patil S L, Chougule M A, Achary S N and Patil V B 2011 *Int. J. Polym. Mater.* **60** 244
[38] Xia H and Wang Q 2002 *Chem. Mater.* **14** 2158
[39] Andrés E S, Toledano-Luque M, Prado A del, Navacerrada M A, Mártil I and González-Díaz G 2005 *J. Vac. Sci. Technol.* A **23** 1523
[40] Hussain A A, Pal A R, Bailung H, Chutia J and Patil D S 2012 *Plasma Chem. Plasma Process.* **32** 817
[41] Li X, Wang D, Luo Q, An J, Wang Y and Cheng G 2008 *J. Chem. Technol. Biotechnol.* **83** 1558
[42] Luca D and Hsu L S 2003 *J. Optoelectron. Adv. Mater.* **5** 835
[43] Bian C, Yu Y and Xue G 2007 *J. Appl. Polym. Sci.* **104** 21
[44] Ameen S, Akhtar M S, Kim Y S and Shin H-S 2011 *Fabrication, Doping and Characterization of Polyaniline and Metal Oxides: Dye Sensitized Solar Cells* in *Solar Cells—Dye-Sensitized Devices* (Rijeka: Intech) chapter 5
[45] Begum N S and Ahmed H M F 2008 *Bull. Mater. Sci.* **31** 43
[46] Sze M 1981 *Physics of Semiconductor Devices* (New York: Wiley)
[47] Gümüş A, Türüt A and Yalçin N 2002 *J. Appl. Phys.* **91** 245
[48] Tung R T 1992 *Phys. Rev.* B **45** 13509
[49] Tung R T, Levi A F J, Sullivan J P and Schrey F 1991 *Phys. Rev. Lett.* **66** 72
[50] Dökme İ, Altindal Ş and Bülbül M M 2006 *Appl. Surf. Sci.* **252** 7749
[51] Cheong K Y, Moon J H, Kim H J, Bahng W and Kim N-K 2008 *J. Appl. Phys.* **103** 084113
[52] Chiu F-C, Chou H-W and Lee J Ya-min 2005 *J. Appl. Phys.* **97** 103503
[53] Mukherjee A, Victor P, Parui J and Krupanidhi S B 2007 *J. Appl. Phys.* **101** 034106